arXiv:0805.3763v2 [hep-ph] 5 Sep 2008

DESY–08–063
CPHT–RR025.0408

Z and $W^{\pm}$ production associated with quark-antiquark pair in k_T-factorization at the LHC

Michal Deák[1], Florian Schwennsen[2]

[1] *DESY, Hamburg, Notkestrasse 85, D–22607 Hamburg, Germany*
[2] *Centre de Physique Théorique, École Polytechnique, F–91128 Palaiseau, France*

Abstract

We calculate and analyze Z and $W^{\pm}$ production in association with quark-antiquark pair in k_T-factorization. Numerical calculations are performed using the Monte Carlo generator CASCADE for proton proton collisions at LHC energy. We compare total and differential cross sections calculated in k_T-factorization approach with total differential cross sections obtained in LO and NLO calculations in collinear factorization approach. We provide strong evidence that some of the effects of the NLO and even higher order collinear calculation are already included in the LO k_T-factorization calculation.

1 Introduction

In the following years new discoveries are expected at the LHC concerning physics within the Standard Model and beyond it. The discovery of the Higgs boson and exclusion or affirmation of possible extensions or alternatives to the Standard Model will be of special interest. To be able to measure the proposed signals of processes which open the access to new physics a very good understanding of the detectors and their responses to produced particles will be needed. An accurate calibration of particle detectors could be achieved by using processes with well known cross sections in which particles with well known properties are produced. A calibration of LHC detectors using W or Z signals is proposed in several publications [1]. Moreover, the W or Z production is important because it plays a significant role in background processes connected to Higgs production. Another

experimental motivation is provided by the possibility to measure the luminosity via Z boson production [2].

At the Tevatron collider W/Z production takes place at a typical $x = \sqrt{M_W^2/s} \approx 0.04$ and hence is dominated by scattering of quarks. Because of the much higher energy, proton scattering at LHC will allow smaller proton energy fractions and will be dominated by gluon scattering.

The W mass provides a hard scale and allows a perturbative calculation of the hard matrix element. The resummation of large logarithms of the form $[\alpha_s \ln(\mu^2/\Lambda^2_{\text{QCD}})]^n$ (where $\mu^2 \sim M_W^2$, $\mu^2 \gg \Lambda^2_{\text{QCD}}$) can be performed in the framework of the Dokshitzer-Gribov-Lipatov-Altarelli-Parisi (DGLAP) equation [3], leading to the collinear factorization into conventional parton densities and a hard scattering matrix element. While in the conventional collinear approach the longitudinal momentum fraction is considered to be dominant, such that the transverse momenta of the partons can be neglected as well as their virtualities, at small x the transverse momenta entering the hard matrix element should become relevant.

At the LHC the larger center of mass energy allows W/Z production at even smaller x such that the production of particles will be dominated by gluon-gluon fusion. Moreover, in this situation we have to deal with two different large scales ($s \gg \mu^2 \gg \Lambda^2_{\text{QCD}}$) and logarithms of the form $[\alpha_s \ln(1/x)]^n$ arise which have to be resummed. This is realized by the leading logarithmic (LL) Balitsky-Fadin-Kuraev-Lipatov (BFKL) equation [4] or the Ciafaloni-Catani-Fiorani-Marchesini (CCFM) evolution equation [5] which additionally resums terms of the form $[\alpha_s \ln(\mu^2/\Lambda^2_{\text{QCD}})]^n$ and $[\alpha_s \ln(\mu^2/\Lambda^2_{\text{QCD}}) \ln(1/x)]^n$. Just as for DGLAP, it is possible to factorize the cross section into a convolution of process-dependent hard matrix elements with universal parton distributions. But as the virtualities and transverse momenta are no longer ordered (as it is the case in DGLAP evolution), the matrix elements have to be taken off-shell, and the convolution has to be made also over transverse momenta with the so-called *unintegrated parton densities*. This factorization scheme is called *k_T-factorization* [6, 7] or *semi-hard approach* [8] and will be used in this work.

There is also the notion of *transverse momentum dependent* (TMD) parton distributions [9]. But although in these approaches the transverse momentum of the parton is taken into account as well, this is only the case on the side of the parton density. The matrix element is calculated with incoming on-shell partons, and transversal momenta of the incoming partons are neglected. It has been shown [10] that factorization within this approach is violated beyond NLO. In case of the k_T-factorization approach used in this work this is also expected. Indeed, it is well known that in the BFKL approach beyond NLO multiple gluon exchange in the t-channel has to be taken into account.

In this paper we calculate and analyze Z and W production associated with two quark jets provided by gluon-gluon fusion in k_T-factorization. We assume quasi-multi-Regge-kinematics (QMRK) where the cluster of W/Z and the two quarks is well separated in rapidity from the proton remnants while the kinematics within that cluster is considered without any further assumption. In particular, we take into account the mass of the quarks. In this kinematic regime a gauge independent off-shell matrix element can be extracted due to high energy factorization. A similar calculation has been done in [11],

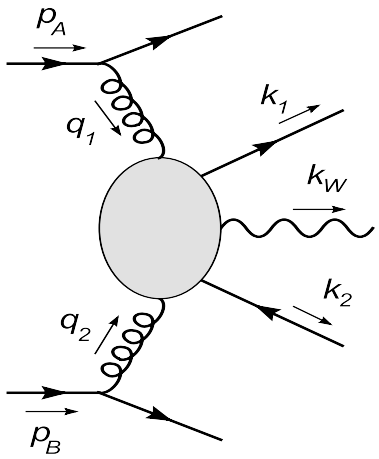

Figure 2.1: Labeling and flow of momenta of the process $pp \to q\,(W/Z)\,\bar{q}\,X$.

where the authors calculated photon (instead of Z/W) production in the same framework. We calculated the matrix element independently and extended it to massive gauge bosons. In our work on massive gauge bosons production we especially focus on the predictions for LHC and compare with a collinear factorization based calculation.

When this paper was in preparation, we learned about another group [12] working on this process as well using the same theoretical approach, but laying more emphasis on confronting the theoretical predictions with experimental data and examining the role of quark contributions.

The paper is organized in the following way: In section 2 we describe notation, kinematics of the process and the calculation of the matrix element. In section 3 we present numerical results obtained from a calculation using the Monte Carlo generator CASCADE [13], where the matrix element squared was implemented. In section 4 we summarize the results and offer conclusions.

2 Kinematics of Z/W production and calculation of the hard matrix element

We label the 4-momenta of incoming hadrons with masses m_A and m_B by p'_A and p'_B, respectively. In the center of mass system they can be expressed in terms of invariant light like vectors p_A and p_B

$$p'_A = p_A + \frac{m_A^2}{s} p_B, \qquad p'_B = p_B + \frac{m_B^2}{s} p_A. \tag{2.1}$$

In the case of protons at the LHC we have $m_A^2 = m_B^2 = m_p^2$ which satisfies the relation $\frac{m_p^2}{s} \ll 1$. Therefore, we can neglect the masses in Eqs. (2.1) and use $p_{A,B}$ instead of $p'_{A,B}$.

It is convenient to use Sudakov decomposition for all momenta present in the calculation

(see also Fig. 2.1[1]) by decomposing them into components proportional to p_A and p_B, and a remainder perpendicular to both of them

$$k_i = \alpha_i p_A + \beta_i p_B + k_{i\perp}, \tag{2.2}$$

where $i \in \{1, 2, W(Z)\}$ for outgoing particles, and

$$q_1 = \alpha p_A + \beta_{q_1} p_B + q_{1\perp}, \qquad q_2 = \alpha_{q_2} p_A + \beta p_B + q_{2\perp} \tag{2.3}$$

for the gluons entering the hard matrix element. It is also convenient to introduce Euclidean two dimensional vectors $\vec{k}_i$ and $\vec{q}_j$ which satisfy the relations $\vec{k}_i^2 = -k_{i\perp}^2 \geq 0$ and $\vec{q}_j^2 = -q_{j\perp}^2 \geq 0$.

In QMRK we have

$$\alpha \gg \beta_{q_1}, \qquad q_1^2 = -\vec{q}_1^2 = t_1, \tag{2.4}$$

$$\beta \gg \alpha_{q_2}, \qquad q_2^2 = -\vec{q}_2^2 = t_2, \tag{2.5}$$

$$\alpha_i \beta_i = \frac{m_i^2 + \vec{k}_i^2}{s}, \tag{2.6}$$

where $i \in \{1, 2, W(Z)\}$, and m_i are the corresponding masses of outgoing particles. The invariants t_1 and t_2 describe the momentum transfer between the cluster formed by the quarks and the W (Z) boson on one hand and the incoming protons on the other hand. Due to the strong ordering in α and β one can neglect terms proportional to β_{q_1} and α_{q_2} in the calculation.

It is useful to introduce a set of Mandelstam variables describing the system

$$\hat{s} = (q_1 + q_2)^2 = \alpha\beta s - (\vec{q}_1 + \vec{q}_2)^2, \tag{2.7a}$$

$$\hat{s}_1 = (k_1 + k_W)^2, \qquad \hat{s}_2 = (k_2 + k_W)^2, \tag{2.7b}$$

$$\hat{t}_1 = (q_1 - k_1)^2, \qquad \hat{t}_2 = (q_2 - k_2)^2, \tag{2.7c}$$

$$\hat{u}_1 = (q_1 - k_2)^2, \qquad \hat{u}_2 = (q_2 - k_1)^2, \tag{2.7d}$$

related by

$$\hat{u}_1 + \hat{t}_2 + \hat{s} = t_1 + t_2 + m_2^2 + \hat{s}_1, \qquad \hat{u}_2 + \hat{t}_1 + \hat{s} = t_1 + t_2 + m_1^2 + \hat{s}_2. \tag{2.8}$$

It is convenient to introduce transverse masses defined by

$$m_{i\perp} = \sqrt{m_i^2 + \vec{k}_i^2}, \qquad m_{q\perp} = \sqrt{\hat{s} + (\vec{q}_1 + \vec{q}_2)^2}, \tag{2.9}$$

and longitudinal momentum fractions of the produced particles $x_i = \frac{\alpha_i}{\alpha}$. Combining these relations with Eqs. (2.6, 2.7) one finds that – in the end – the matrix element of W or Z production associated with a quark-antiquark pair can be expressed in terms of independent Mandelstam variables defined in Eqs. (2.7), transverse masses and variables $x_{1,2,W(Z)}$.

[1] These and the following diagrams were drawn in JaxoDraw [14].

In the k_T-factorization formalism the hadronic and partonic cross section are related as follows:

$$d\sigma(pp \to q\,(W/Z)\,\bar{q}\,X) = \int \frac{d\alpha}{\alpha} \int d\vec{q}_1^{\,2} \int \frac{d\phi_1}{2\pi} \mathcal{A}(\alpha, \vec{q}_1^{\,2}, \mu^2) \times \int \frac{d\beta}{\beta} \int d\vec{q}_2^{\,2} \int \frac{d\phi_2}{2\pi} \mathcal{A}(\beta, \vec{q}_2^{\,2}, \mu^2) d\hat{\sigma}(g^* g^* \to q\,(W/Z)\,\bar{q}), \quad (2.10)$$

where $\mathcal{A}$ is the unintegrated gluon density in a proton and $\phi_{1,2}$ is the angle of $\vec{q}_{1,2}$ with respect to some fixed axis in the azimuthal plane. The argument μ^2 of unintegrated gluon densities is the factorization scale. The partonic cross section is denoted by $d\hat{\sigma}$.

Since the incoming gluons of the matrix element entering this partonic cross section are off-shell, the calculation differs from that of a hard matrix element in the collinear approach significantly. To guarantee gauge invariance, the process with off-shell incoming particles has to be embedded into the scattering of on-shell particles. The extracted off-shell matrix element is of course independent of the specific choice of the particles in which the scattering process is embedded. Therefore, we replace the protons by quarks for the calculation of the hard matrix element. All diagrams for the discussed process are shown in Fig. 2.2.

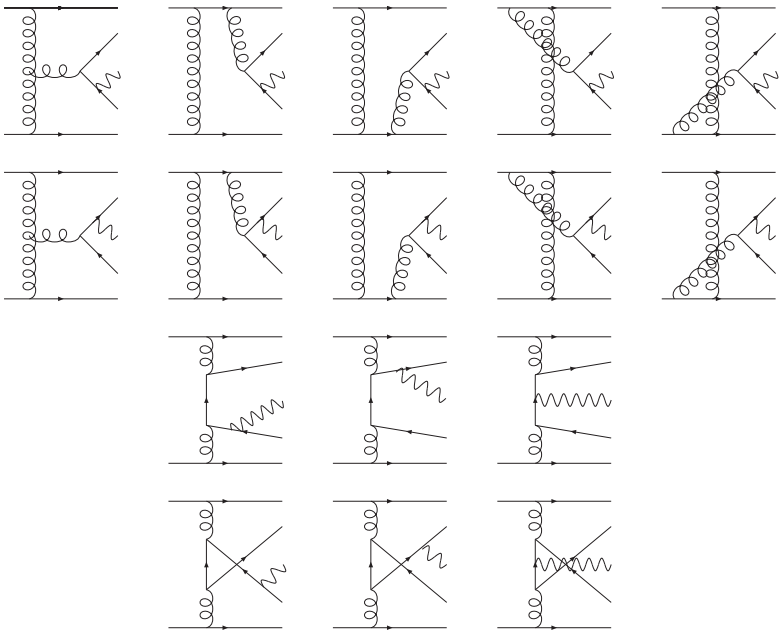

Figure 2.2: Full set of diagrams contributing to W/Z production via off-shell gluon-gluon fusion.

The first two rows of Fig. 2.2 include also non-factorizing ('non-resonant') diagrams which factorize only in the sum. To make this factorization apparent already at this level, one can sum up the different diagrams of one gluon production in quark-quark scattering

leading to one effective diagram with an effective vertex (see Fig. 2.3). By working in Feynman gauge one obtains the well known Lipatov vertex [15]:

$$\Gamma^{\nu}_{\sigma\tau}(q_1,q_2) = \frac{2p_{A\tau}p_{B\sigma}}{s}\left(\frac{2t_1+m^2_{q\perp}}{\beta s}p^{\nu}_A - \frac{2t_2+m^2_{q\perp}}{\alpha s}p^{\nu}_B - (q_{1\perp}-q_{2\perp})^{\nu}\right). \tag{2.11}$$

It can be shown that this vertex obeys the Ward identity. By this procedure, the first two rows of Fig. 2.2 are each replaced by just one diagram.

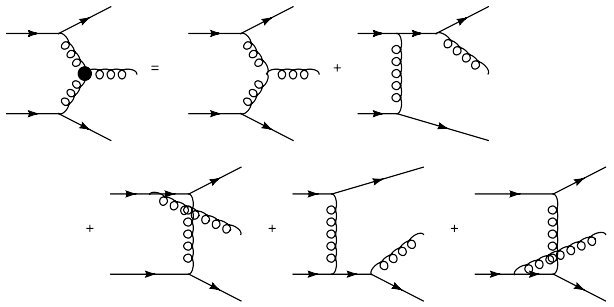

Figure 2.3: Diagrams contributing to the Lipatov vertex.

Strong ordering of Mandelstam variables s and $t_{1,2}$ allows us to make a simplification of the coupling of gluons to incoming quarks. By neglecting the exchanged momentum in the vertex, we get an eikonal vertex which does not depend on the spin of the particle coupled to gluon and preserves its spin. In detail, it reads

$$-i\bar{u}(\lambda_1', p_A - q_1)\gamma^{\mu}u(\lambda_1, p_A) \quad \longrightarrow \quad -2ip^{\mu}_A\delta_{\lambda_1',\lambda_1}. \tag{2.12}$$

With the help of Eq. (2.12) it is possible to remove the external quark lines and attach so-called 'non-sense' polarizations to the incoming gluons:

$$\epsilon^{\mu}_{q_1} = \frac{\sqrt{2}\,p^{\mu}_A}{\sqrt{s}}, \qquad\qquad \epsilon^{\nu}_{q_2} = \frac{\sqrt{2}\,p^{\nu}_B}{\sqrt{s}}. \tag{2.13}$$

Instead of Feynman gauge, one can choose an appropriate axial gauge [6] $n\cdot A = 0$ with the gauge vector

$$n^{\mu} = ap^{\mu}_A + bp^{\mu}_B \quad \text{with} \quad a,b \in \mathbb{C}. \tag{2.14}$$

The contraction of the eikonal coupling (2.12) with the gluon polarization tensor in this gauge

$$d^{(n)}_{\mu\nu}(q) = -g_{\mu\nu} + \frac{n_{\mu}q_{\nu}+q_{\mu}n_{\nu}}{nq} - n^2\frac{q_{\mu}q_{\nu}}{(nq)^2} \tag{2.15}$$

then reads

$$p^{\mu}_A d^{(n)}_{\mu\nu}(q_1) = \frac{q_{1\perp\nu}}{\alpha}, \qquad\qquad p^{\mu}_B d^{(n)}_{\mu\nu}(q_2) = \frac{q_{2\perp\nu}}{\beta}. \tag{2.16}$$

In such a physical gauge the 'non-resonant' diagrams vanish since the direct connection of two eikonal couplings gives $p_A^\mu d_{\mu\nu}^{(n)} p_B^\nu = 0$ (in other words: the Lipatov vertex is to be replaced by the usual three gluon vertex).

In the case of heavy quark production the polarization sum for the s-channel gluon reduces to its Feynman gauge analogue $-g_{\mu\nu}$ due to the heavy flavor current conservation. The same simplification takes place in our calculation. Nevertheless, we have to stress that in general the polarization sum stays in its complex form. Of course, both ways to calculate the matrix element are equivalent due to gauge invariance.

The sum over the physical polarizations η of the W boson reads

$$\sum_\eta \epsilon^\mu(\eta, k_W)\epsilon^{*\nu}(\eta, k_W) = -g^{\mu\nu} + \frac{k_W^\mu k_W^\nu}{m_W^2}. \tag{2.17}$$

It is equivalent to replace the polarization sum by

$$\sum_\eta \epsilon^\mu(\eta, k_W)\epsilon^{*\nu}(\eta, k_W) \quad \to \quad -g^{\mu\nu}, \tag{2.18}$$

and to add also the contribution of the Goldstone boson emission diagrams, where the W boson is replaced by a Goldstone boson with mass m_W. This is in analogy of using the Feynman-t'Hooft gauge instead of the unitary gauge. We have calculated the squared matrix element in both ways as a crosscheck.

Expressions for the single diagrams in Fig. 2.2 – where the first diagrams are already combined using the Lipatov vertex of Eq. (2.11) – are listed here (the hat marks contraction with Dirac-matrices):

$$\begin{aligned}
\mathcal{M}_{1\mu\nu}^{ab} &= -ig_w g_s^2 K_{W/Z}\ \bar{u}[t^b, t^a]\frac{\hat{\Gamma}_{\mu\nu}(q_1, q_2)}{\hat{s}}\frac{-\hat{k}_2 - \hat{k}_W + m_1}{\hat{s}_2 - m_1^2}\hat{\epsilon}(v_q - a_q\gamma^5)v,\\
\mathcal{M}_{2\mu\nu}^{ab} &= -ig_w g_s^2 K_{W/Z}\ \bar{u}\hat{\epsilon}(v_q - a_q\gamma^5)\frac{\hat{k}_1 + \hat{k}_W + m_2}{\hat{s}_1 - m_2^2}[t^b, t^a]\frac{\hat{\Gamma}_{\mu\nu}(q_1, q_2)}{\hat{s}}v,\\
\mathcal{M}_{3\mu\nu}^{ab} &= -ig_w g_s^2 K_{W/Z}\ \bar{u}t^a\gamma_\mu\frac{\hat{k}_1 - \hat{q}_1 + m_1}{\hat{t}_1 - m_1^2}t^b\gamma_\nu\frac{-\hat{k}_2 - \hat{k}_W + m_1}{\hat{s}_2 - m_1^2}\hat{\epsilon}(v_q - a_q\gamma^5)v,\\
\mathcal{M}_{4\mu\nu}^{ab} &= -ig_w g_s^2 K_{W/Z}\ \bar{u}\hat{\epsilon}(v_q - a_q\gamma^5)\frac{\hat{k}_1 + \hat{k}_W + m_2}{\hat{s}_1 - m_2^2}t^a\gamma_\mu\frac{\hat{q}_2 - \hat{k}_2 + m_2}{\hat{t}_2 - m_2^2}t^b\gamma_\nu v,\\
\mathcal{M}_{5\mu\nu}^{ab} &= -ig_w g_s^2 K_{W/Z}\ \bar{u}t^a\gamma_\mu\frac{\hat{k}_1 - \hat{q}_1 + m_1}{\hat{t}_1 - m_1^2}\hat{\epsilon}(v_q - a_q\gamma^5)\frac{\hat{q}_2 - \hat{k}_2 + m_2}{\hat{t}_2 - m_2^2}t^b\gamma_\nu v,\\
\mathcal{M}_{6\mu\nu}^{ab} &= -ig_w g_s^2 K_{W/Z}\ \bar{u}\hat{\epsilon}(v_q - a_q\gamma^5)\frac{\hat{k}_1 + \hat{k}_W + m_2}{\hat{s}_1 - m_2^2}t^b\gamma_\nu\frac{\hat{q}_1 - \hat{k}_2 + m_2}{\hat{u}_1 - m_2^2}t^a\gamma_\mu v,\\
\mathcal{M}_{7\mu\nu}^{ab} &= -ig_w g_s^2 K_{W/Z}\ \bar{u}t^b\gamma_\nu\frac{\hat{k}_1 - \hat{q}_2 + m_1}{\hat{u}_2 - m_1^2}t^a\gamma_\mu\frac{-\hat{k}_2 - \hat{k}_W + m_1}{\hat{s}_2 - m_1^2}\hat{\epsilon}(v_q - a_q\gamma^5)v,\\
\mathcal{M}_{8\mu\nu}^{ab} &= -ig_w g_s^2 K_{W/Z}\ \bar{u}t^b\gamma_\nu\frac{\hat{k}_1 - \hat{q}_2 + m_1}{\hat{u}_2 - m_1^2}\hat{\epsilon}(v_q - a_q\gamma^5)\frac{\hat{q}_1 - \hat{k}_2 + m_2}{\hat{u}_1 - m_2^2}t^a\gamma_\mu v,
\end{aligned} \tag{2.19}$$

with the short hand notations $\bar{u} \equiv \bar{u}(\lambda, k_1)$, $v \equiv v(\lambda', k_2)$, $\hat{\epsilon} \equiv \hat{\epsilon}(\eta, k_W)$, and where η, λ and λ' label the helicity/ spins of the corresponding particles. Color factors are represented by Gell-Mann matrices t^a, t^b. The factors v_q, a_q and $K_{W/Z}$ encode the W and Z coupling. For W boson we have $v_q = a_q = 1$ and $K_W = V_{ud}\frac{1}{2\sqrt{2}}$, where V_{ud} is the corresponding element of Cabibbo-Kobayashi-Maskawa matrix. For Z we have $a_u = \frac{1}{2}$, $v_u = \frac{1}{2} - \frac{4}{3}\sin^2\theta_W$ and $a_d = -\frac{1}{2}$, $v_d = -\frac{1}{2} + \frac{2}{3}\sin^2\theta_W$ and $K_Z = \frac{1}{2\cos\theta_W}$, where θ_W is the Weinberg angle. In the latter case m_1 equals m_2, and m_W is replaced by m_Z.

If we make use of the Eq. (2.18) to replace the polarization sum, one has to add diagrams and corresponding amplitudes with Goldstone bosons with couplings

$$-ig_w K_{W/Z}\Big(\frac{m_2 - m_1}{m_{W/Z}}\, v_q - \frac{m_1 + m_2}{m_{W/Z}}\, a_q\gamma^5\Big). \tag{2.20}$$

Finally, the square of the amplitude averaged over initial helicities and colors of gluons and summed over spins/ helicities and colors of final particles can be written as

$$\frac{1}{4}\frac{1}{(N_c^2-1)^2}|\mathcal{M}|^2 = \frac{1}{4}\frac{1}{(N_c^2-1)^2}\sum_{\lambda,\lambda',\eta,a,b}\mathrm{Tr}_{\mathrm{color}}\left\{\left|\sum_{i=1}^{8}\epsilon^{\mu}_{q_1}\epsilon^{\nu}_{q_2}\mathcal{M}^{ab}_{i\mu\nu}\right|^2\right\}. \tag{2.21}$$

By evaluating the traces over the products of Gell-Mann color matrices, one encounters two possible cases of color factors

$$\mathrm{Tr}\{t^a t^b t^a t^b\} = -\frac{1}{4}\frac{N_c^2-1}{N_c}, \qquad \mathrm{Tr}\{t^a t^b t^b t^a\} = \frac{1}{4}\frac{(N_c^2-1)^2}{N_c}, \tag{2.22}$$

where $N_c = 3$ is the number of colors.

Finally, the expression for the partonic off-shell cross section appearing in Eq. (2.10) to calculate the hadronic cross section is

$$\begin{aligned} d\hat{\sigma}(g^*g^* \to q\,(W/Z)\,\bar{q}\,) =& (2\pi)^4\delta^{(4)}\left(q_1 + q_2 - k_1 - k_2 - k_{W/Z}\right)\times \\ &\times \frac{1}{2\alpha\beta s}\frac{\alpha^2\beta^2 s^2}{t_1 t_2}\frac{1}{4}\frac{1}{(N_c^2-1)^2}|\mathcal{M}|^2\prod_{i\in\{1,2,W(Z)\}}\frac{d^3k_i}{(2\pi)^3 2E(k_i)}. \end{aligned} \tag{2.23}$$

The origin of the specific form of the flux factor and prefactor $\frac{\alpha^2\beta^2 s^2}{t_1 t_2}$ is formulated in [6, 7]. We summarize the most relevant aspects here. An important feature of the whole calculation is that it is possible to recover the result obtained in collinear factorization by neglecting the transverse momenta of the gluons when they enter the hard matrix element and instead integrate over them only in the gluon densities. Due to factorization it is possible to keep this connection not only for the full cross section, but also for gluon densities and hard matrix element separately as well, provided that the explicit manifestations of the factorization formulae are phrased.

The key point is the observation that

$$\left\langle 2\frac{q_{1\perp\mu}q_{1\perp\nu}}{q_{1\perp}^2}\right\rangle_{\phi_1} = -g^{\perp}_{\mu\nu} = \left\langle 2\frac{q_{2\perp\mu}q_{2\perp\nu}}{q_{2\perp}^2}\right\rangle_{\phi_2}. \tag{2.24}$$

As shown in Eqs. (2.14-2.16), in an appropriate gauge the polarization sum $\frac{2p_{A\mu}p_{B\nu}}{s}$ can be replaced by $\frac{2q_{1\perp\mu}q_{2\perp\nu}}{\alpha\beta s}$. Since in this gauge one has to deal with exactly the same diagrams as in the on-shell calculation, by dressing the off-shell matrix element squared with the prefactor $\frac{\alpha^2\beta^2 s^2}{t_1 t_2}$ and performing the averaging over azimuthal angles of the 'incoming' gluons, followed by taking the limit $t_1, t_2 \to 0$, one gets the collinear limit of the matrix element squared. The flux factor for off-shell gluons is defined as for on-shell gluons with $\frac{1}{2\alpha\beta s}$. As the matrix element is gauge invariant, this connection remains valid when one performs the current calculation in a different gauge.

Due to the off-shellness of the incoming gluons and the three particle final state the final result of the matrix element squared is rather lengthy. For that reason, we calculated it independently and in different ways. One calculation followed directly the derivation above using Feynman gauge for the gluons, and has been performed using MATHEMATICA. A second calculation written in FORM [16,17] used an axial gauge as described above such that the Lipatov vertices in (2.19) are to be replaced by standard three-gluon-vertices. Moreover this second method used the method of orthogonal amplitudes, described in [18], which affects the fermionic part of the matrix element and with which one is able to treat the matrix element squared in a more compact way.[2]

For this second method a few technical details are elaborated in the remainder of this section. The method of orthogonal amplitudes is based on expressing a generic amplitude $\widetilde{\mathcal{M}}$ (with one quark line) in terms of a set of four independent operators $\hat{O}_i,\ i \in \{1,..,4\}$, which satisfy orthogonality relations $\mathrm{Tr}\{\hat{O}_i(\hat{k}_2 - m_2)\overline{\hat{O}_j}(\hat{k}_1 + m_1)\} = \|\hat{O}_i\|^2\delta_{ij}$ for any possible i and j, where $\|\hat{O}_i\|$ is the "norm" of the operator $\hat{O}_i$. The projection of $\widetilde{\mathcal{M}}$ by an operator $\hat{O}_i$ is performed in the following way

$$\widetilde{\mathcal{M}}^i = \frac{1}{\|\hat{O}_i\|}\sum_{\lambda,\lambda'}\widetilde{\mathcal{M}}\,\bar{v}(\lambda', k_2)\overline{\hat{O}_i}u(\lambda, k_1). \tag{2.25}$$

The matrix element squared then has the following form

$$\sum_{\lambda,\lambda'}|\widetilde{\mathcal{M}}|^2 = \sum_i |\widetilde{\mathcal{M}}^i|^2. \tag{2.26}$$

In our case the matrix element consists of up to five Dirac-matrices (neglecting γ^5), after squaring one has to evaluate traces of up to twelve of them. In contrast the method of orthogonal amplitudes leads only to traces of up to eight Dirac-matrices.

If one wants to consider also the Z or $W^\pm$ coupling in the Feynman diagram, one encounters a technical problem connected with the appearance of the Dirac-matrix γ^5 in the expression for the amplitude, leading to terms which include Levi-Civita tensors which later cancel. To avoid this complication, one can split the expression for the amplitude into two parts, one which does not include γ^5 and the other one which does (to separate the vector and axial part of the Z or W boson coupling). For the part with γ^5 one uses a base of operators $\hat{O}_i\gamma^5$. It is easy to check that they satisfy the same orthogonality relation

[2] We also have cross-checked numerically our results for the case of a produced photon instead of a W/Z boson with those of the authors of [11] whose cooperation we gratefully acknowledge.

like the operators $\hat{O}_i$. One also easily see that projections of amplitudes in which γ^5 occurs do not contain terms with Levi-Civita tensors. In doing so, we extend the method of orthogonal amplitudes in a natural way.

Another complication comes from the presence of color factors in the expressions which are not numbers but matrices. To treat the projections as numbers, it is necessary to separate the Feynman diagrams into three groups according to different color factors, namely

$$\begin{aligned} C_1^{ab} &= t^a t^b - t^b t^a, \\ C_2^{ab} &= t^a t^b, \\ C_3^{ab} &= t^b t^a, \end{aligned} \tag{2.27}$$

which form a vector $C^{ab} = (C_1^{ab}, C_2^{ab}, C_3^{ab})$ (components of C^{ab} are color factors of $\mathcal{M}^{ab}_{(1,2)\mu\nu}$, $\mathcal{M}^{ab}_{(3-5)\mu\nu}$ and $\mathcal{M}^{ab}_{(6-8)\mu\nu}$ correspondingly). One can then build a corresponding vector containing the sums of Feynman diagrams without the color factors $\mathcal{F} = (\mathcal{F}_1, \mathcal{F}_2, \mathcal{F}_3)$ such that

$$\mathcal{M}^{ab} = (C^{ab})^T \mathcal{F}. \tag{2.28}$$

The Lorentz indices have been dropped for simplicity. Using the matrix

$$\mathcal{C}_{ij} = \mathrm{Tr}\{C_i^{ab} C_j^{ba}\}, \tag{2.29}$$

the expression for the square of the matrix element takes the form

$$|\mathcal{M}|^2 = \mathcal{F}^\dagger \mathcal{C} \mathcal{F}, \tag{2.30}$$

where combinations of $\mathcal{F}_i$ and $\mathcal{F}_j^*$ are calculated using the projection method introduced in Eqs. (2.25, 2.26). For the final simplification we have diagonalized the matrix $\mathcal{C}$. After diagonalization of the matrix $\mathcal{C}$ only two diagonal elements remain nonzero. This is expected because the quarks in the final state, in this process, can occur only in two possible color states.

3 Numerical studies

The last missing pieces needed to calculate the hadronic cross section using Eq. (2.10), are the unintegrated gluon densities. As mentioned in the introduction, there are two equations suited to describe the evolution of an unintegrated gluon density, namely BFKL [4] and CCFM [5], respectively. Both have been shown to agree on the leading logarithms in small x [19], but the CCFM evolution is valid in the domain of larger x as well and, moreover, matches in this region with DGLAP. Therefore, we base our numerical studies on an unintegrated gluon density obeying the CCFM equation, which has been implemented in the Monte Carlo generator CASCADE [13]. We also investigate how the results change when using uPDFs generated by a different procedure known as KMR [20].

For this purpose, we implemented the matrix element squared as described above into CASCADE. This implementation will be available in the next version of CASCADE.

We have used the unintegrated parton distribution function (uPDF) CCFM 2003 set 3 for the numerical calculation.

To investigate the calculated matrix element as accurately as possible, we neglect in this first study the effect of hadronization of the final state. We study in detail rapidity and transverse momentum distributions of the produced gauge boson, quark and antiquark which (if one assumes that quarks approximately determine jets) are the most important observables in the experiment.

Furthermore, we compare the k_T-factorization approach to the collinear one. For this purpose, we compare the distributions obtained by our transverse momenta dependent matrix element with distributions obtained from the Monte Carlo generator MCFM [21] which provides a calculation of the same process in the collinear limit. In that case the transverse momenta coming from the evolution are neglected. We also investigate in Sec. 3.3 how the variation of unintegrated parton densities affect the azimuthal angle and transverse momenta distributions.

As an artefact of the perturbative calculation, the results depend on the renormalization scale μ_R and the factorization scale μ_f. In the CCFM formalism the hardest scale is set by the emission angle of the hardest subcollision. It can be expressed in terms of the energy of the subcollision $\mu_f = \sqrt{\hat{s} + (\vec{q}_1 + \vec{q}_2)^2}$. For the comparison with collinear factorization calculations we have used as renormalization scale $\mu_R = m_Z$ in k_T-factorization calculation and in collinear calculation as well. We have also investigated other possible choices (see subsection 3.3).

3.1 Comparison with LO collinear calculation

Our calculation of the hard matrix elements includes $W^{\pm}$ and Z production in association with all possible quark-antiquark channels in gluon gluon fusion. Since the basic structure of all these matrix elements is very similar, we present results only for the typical case of $Zb\bar{b}$ production at LHC energies of $\sqrt{s} = 14$TeV. The mass of the b-quark used is $m_b = 4.62$ GeV. For the collinear factorization calculations we use the parton densities CTEQ6L1 [22].

The total cross sections are comparable in magnitude, though they differ considerably: 0.406 nb in k_T-factorization and 0.748 nb in collinear factorization. The difference of total cross sections stems from the different behavior at low transversal momenta of final state particles (discussed later in this section) where contributions from transversal momenta of the initial state gluons play a significant role. It can be seen that by applying a cut on the transversal momentum of the Z boson $p_{Z\perp} > 50\,\text{GeV}$ the difference of the total cross sections becomes smaller. With this additional cut one obtains cross sections of 0.118 nb in k_T-factorization and 0.141 nb in LO collinear calculation.

The total cross sections for other final states of interest are given in Tab. 3.1.

The transverse momentum and rapidity distributions of the vector boson are shown in Fig. 3.1 and 3.2, respectively. The comparison of the k_T-factorization approach to the collinear shows that they agree in transversal momentum distributions of Z at high values of this quantity. This is no surprise, since at high $p_{Z\perp}$ the contribution from initial state gluon transverse momenta is expected to become small.

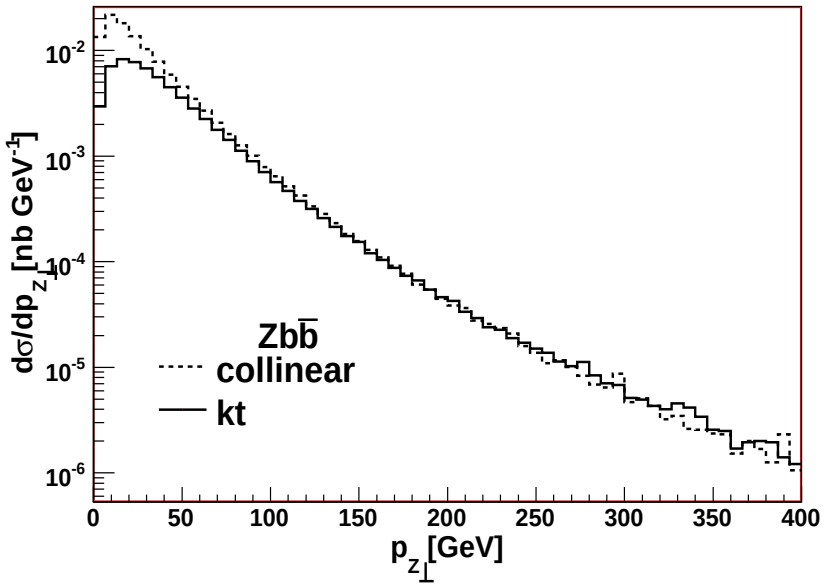

Figure 3.1: Transverse momentum distributions of the produced Z gauge bosons. Calculation with massive b-quarks. Both calculations are in LO of perturbation series.

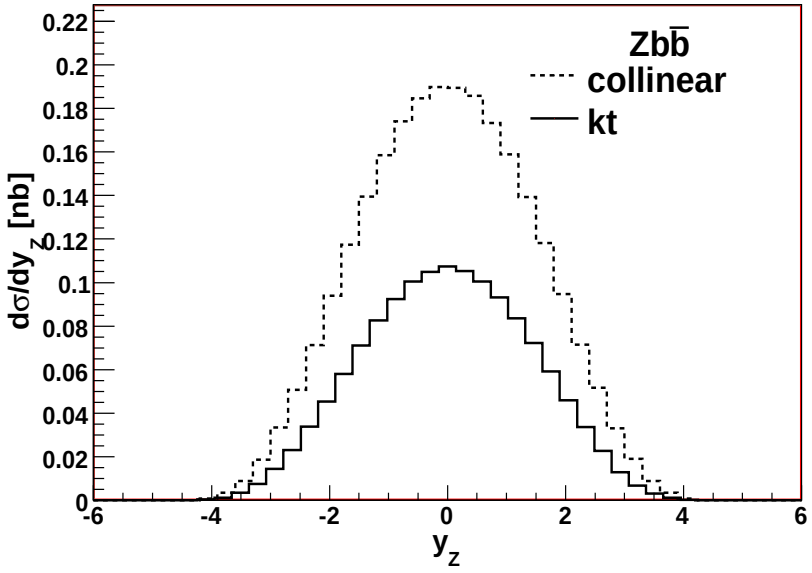

Figure 3.2: Rapidity distribution of the produced Z gauge bosons. Calculation with massive b-quarks. Both calculations are in LO of perturbation series.

final state	$Zc\bar{c}$	$Zb\bar{b}$	$Zt\bar{t}$	$W^+s\bar{c}$, $W^-c\bar{s}$
σ_{tot} [nb]	0.430	0.406	$0.525 \cdot 10^{-3}$	1.92

Table 3.1: Total cross sections for different final states, calculated in k_T-factorization using CASCADE.

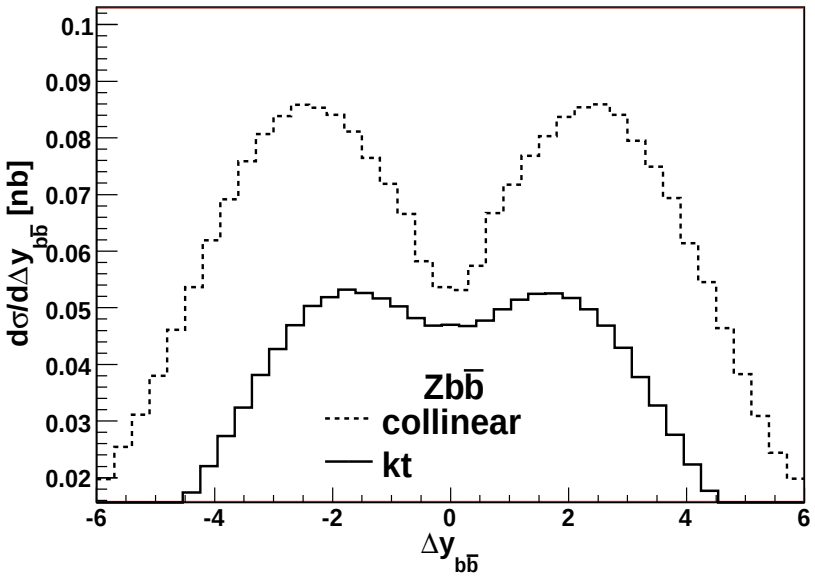

Figure 3.3: Distributions of the rapidity distance between quark and antiquark. Calculation with massive b-quarks. Both calculations are in LO of perturbation series.

The rapidity distributions of the Z show a similar behavior, except for the overall normalization (Fig. 3.2).

To elaborate the difference between k_T- and collinear factorization, we investigate more exclusive observables, like the cross section differential in rapidity distance between quark and antiquark (Fig. 3.3). Both calculations show a two peak structure with a minimum at zero rapidity, but the k_T-factorization result has a considerably shallower minimum. The minimum in the case of the collinear calculation gets shallower – bringing together both calculations – when one again applies a cut on $p_{Z\perp} > 50\,\text{GeV}$ as one can see in Fig. 3.4.

In the distribution of the azimuthal angular distance of Z and $\max(p_{b,\perp}, p_{\bar{b},\perp})$ (Fig. 3.5) we observe that the region from 0 to $\pi/2$ is forbidden within the collinear calculation due to momentum conservation, which is not the case for k_T-factorization. This is caused by the contribution from initial state gluon transversal momentum which allows the transversal momenta of Z, b and $\bar{b}$ to be unbalanced. A larger spread of possible configurations causes that the distribution in the k_T-factorization calculation flattens.

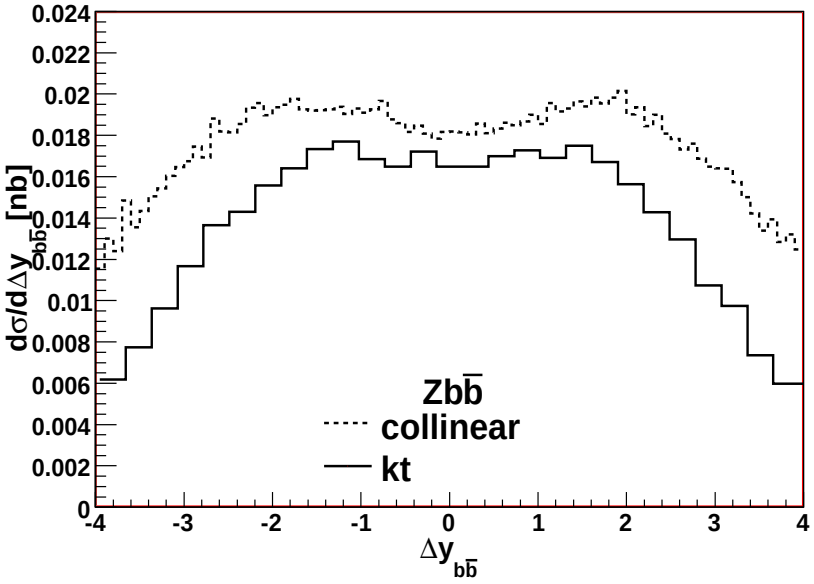

Figure 3.4: Distributions of the rapidity distance between quark and antiquark. Calculation with massive b-quarks. A cut on $p_{Z\perp} > 50\,\mathrm{GeV}$ has been applied.

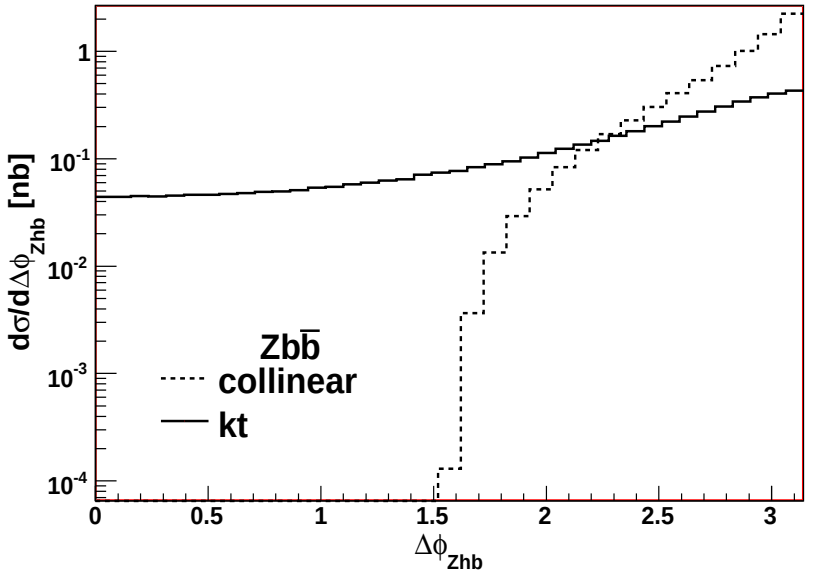

Figure 3.5: Distributions of the distance in azimuthal angle of Z and highest $p_\perp$ quark or antiquark. Calculation with massive b-quarks. Both calculations are in LO of perturbation series.

3.2 Comparison with NLO collinear calculation

In collinear factorization the physical effect of the intrinsic transverse momenta of the initial gluons can not be described until higher order corrections are taken into account. Then additional real emissions lead to off-shell gluons and their transverse momenta. Therefore, the significant differences between a calculation in the collinear factorization framework and k_T-factorization framework shown in the previous section encourage us to compare our LO calculation in k_T-factorization with a NLO collinear calculation, since CCFM evolution includes the high-energy part of the NLO collinear corrections. Since there are two off-shell initial gluons in a k_T-factorized pp-collision, one could even call for a higher order collinear calculation to compare[3].

To compare with a collinear NLO calculation, we use again the Monte Carlo generator MCFM. This Monte Carlo generator provides the process $gg \to Zb\bar{b}$ at NLO only in the massless quark limit. To avoid divergences, additional cuts are applied on transversal momenta of quarks, on the invariant mass of the $b\bar{b}$ pair, and on transversal momenta of a gluon which is produced in diagrams of real NLO corrections. Transversal momenta of produced quark, antiquark and gluon have to satisfy the condition $p_\perp > 4.62\text{GeV}$ (corresponding to the mass of the b-quark). These cuts on quark (antiquark) momenta are automatically applied in MCFM when one is performing a calculation involving massless quarks (antiquarks). We choose the parton density functions set CTEQ6M [22]. The same cuts on transversal momenta of quark and antiquark are then applied in CASCADE as well.

For the total cross sections, we obtain in the NLO collinear factorization calculation 1.04 nb, and in the k_T-factorization calculation 0.429 nb. The difference of the total cross sections in k_T-factorization calculation and the NLO calculation in collinear factorization is of the same origin as the difference between the total cross sections in section 3.1 where comparison of k_T-factorization calculation and NLO calculation in collinear factorization is discussed. This is again illustrated by a cut on $p_{Z\perp} > 50\,\text{GeV}$ diminishing the difference between the cross sections (0.125 nb for the k_T-factorization calculation and 0.165 nb for the NLO calculation in collinear factorization).

The result for the cross sections differential in the transversal momentum of Z can be seen in Fig. 3.6. The cross section changes especially at small $p_{Z\perp}$ (see Fig. 3.7) from LO to NLO calculation, and the difference between collinear calculation and k_T-factorization calculation becomes more pronounced. We observe that the maximum of the distribution in the NLO calculation (MCFM) stays approximately at same value of transversal momenta and the shape of the peak is very different from the one we obtain in k_T-factorization. Nevertheless, the $p_{Z\perp}$ distributions match at very high $p_{Z\perp}$ ($\mathcal{O}(10^2\text{GeV})$).

The rapidity distribution of the Z (Fig. 3.8) shows no major difference in shape in k_T-factorization approach, LO and NLO collinear factorization approach.

[3] Although we argue that already the LO k_T-factorization calculation includes in some sense higher order corrections, one might ask for an extension to NLO. So far k_T-factorization based on CCFM evolution has been formulated only at LO. On the other hand, since the BFKL equation has been calculated at NLO accuracy [23], in the small x regime k_T-factorization can be formulated at NLO accuracy as well [24]. Nevertheless, an implementation into a Monte Carlo generator is still outstanding. Moreover, the calculation of an off-shell $2 \to 3$ process at one loop order is far beyond the scope of this work.

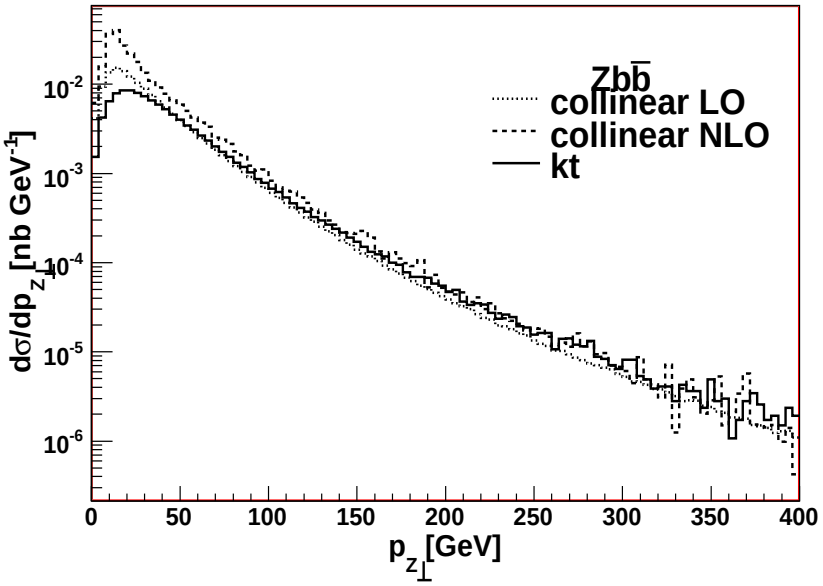

Figure 3.6: Comparison of cross sections differential in transverse momentum of the produced Z gauge boson. Calculation with massless b-quarks. The applied cuts are described in the text.

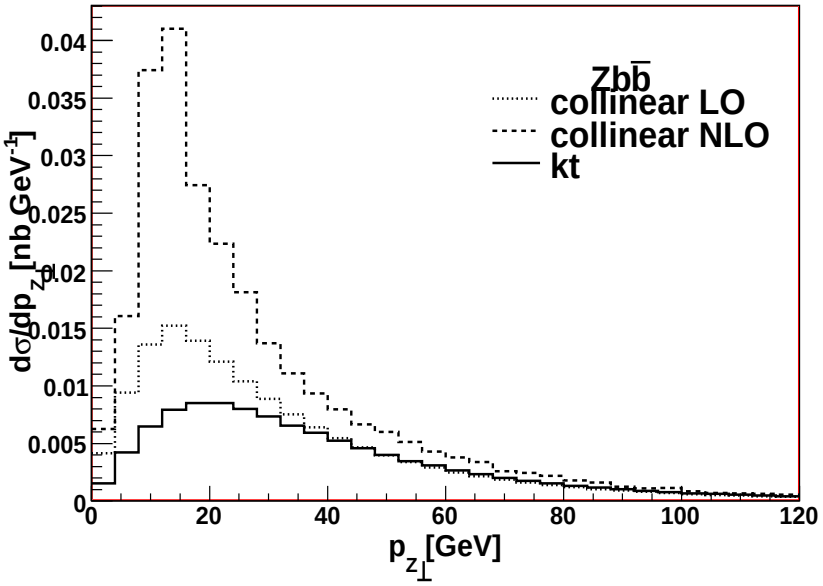

Figure 3.7: Comparison of cross sections differential in transverse momentum of the produced Z gauge boson (linear scale). Calculation with massless b-quarks. The applied cuts are described in the text.

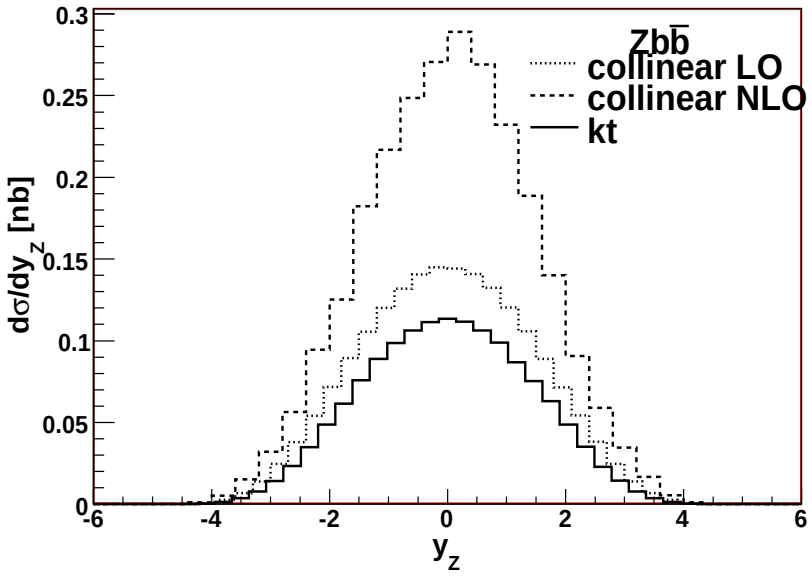

Figure 3.8: Comparison of cross sections differential in rapidity of the produced Z gauge boson (logarithmic scale). Calculation with massless b-quarks. The applied cuts are described in the text.

We consider the cross section differential in the total transversal momentum of the $Zb\bar{b}$ system $p_{Zb\bar{b}\perp}$ in Fig. 3.9. In the NLO collinear calculation a non-zero $p_{Zb\bar{b}\perp}$ is generated by the emission of an additional gluon, while at LO it is always balanced to zero. At low $p_{Zb\bar{b}\perp}$ we see the consequence of the cut on the transverse momenta of the outgoing particles in MCFM (a small gap between 0 GeV and 4.62 GeV in $p_{Zb\bar{b}\perp}$ histogram). Since there are no parton showers or soft gluon re-summation [25] included in the MCFM NLO calculation, one observes a steep rise of the cross section towards zero transverse momentum because the matrix element diverges when approaching $p_{Zb\bar{b}\perp} \to 0\,\text{GeV}$. On the other hand, uPDFs include corrections similar to parton shower effects, treated consistently, which causes the turnover in the cross section of the k_T-factorization calculation. Here, the entire transversal momentum of the $Zb\bar{b}$ system stems from the transversal momenta of initial state gluons. We expect that resummation effects at low values of $p_{Zb\bar{b}\perp}$ would tame the growth of the cross section in collinear factorization and would decrease the difference to k_T-factorization. Interestingly, there is a difference not only at low values of $p_{Zb\bar{b}\perp}$, but also at high values of $p_{Zb\bar{b}\perp}$. The differential cross sections at high $p_{Zb\bar{b}\perp}$ have a similar slope, but differ by a factor of ~ 3. This is contrary to the behavior of distributions of $p_{Z\perp}$ in Figs. 3.6 and 3.1 where at large values of $p_{Z\perp}$ the differential cross sections overlap. For this difference at large $p_{Zb\bar{b}\perp}$ further calculations have to reveal the exact effect of higher order corrections in collinear factorization, keeping in mind that the NLO for this obersvable de facto is the first non trivial order.

The cross section differential in the difference of azimuthal angles of Z and b or $\bar{b}$ quark

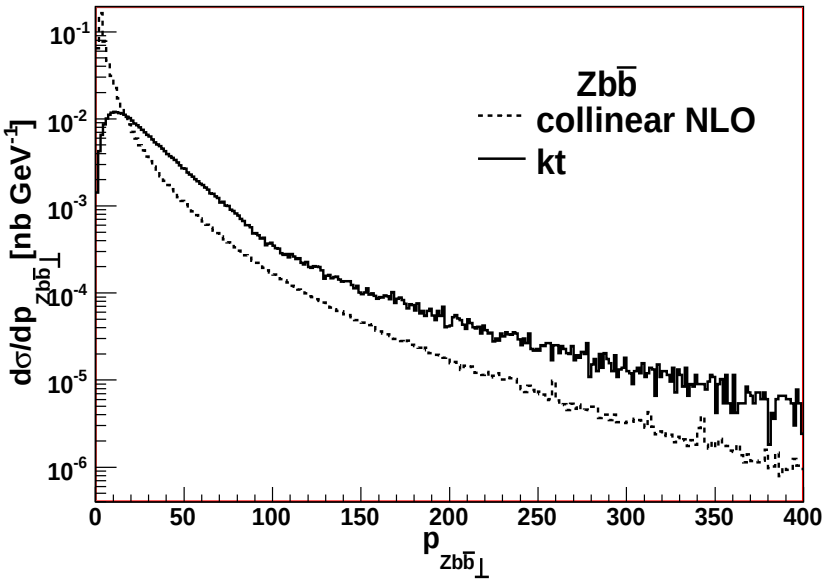

Figure 3.9: Comparison of cross sections differential in the $p_\perp$ of the system $Zb\bar{b}$. Calculation with massless b-quarks. The applied cuts are described in the text.

with higher transversal momentum – $\Delta\phi_{Zhb}$ – is shown in Fig. 3.10. Going from LO to NLO, the collinear calculation reveals a broader distribution like in the k_T-factorization case. Nevertheless, the k_T-factorization result shows a more homogeneous spread of the azimuthal angle distance. This difference origins partly in the difference of the transversal momentum distributions at low values (see Fig. 3.7). A cut on low values ($p_{Z\perp} > 50\,\text{GeV}$) of the transversal momentum of the Z boson results in steeper $\Delta\phi_{Zhb}$ distributions as shown in Fig. 3.11. Still, the k_T-factorization result is flatter than the NLO collinear factorization calculation giving an indication that there is a contribution from the total transversal momentum of the $Zb\bar{b}$ system generated by both uPDFs.

3.3 Variation of the CASCADE results on uPDF and renormalization scale

To estimate the uncertainty coming from the different choices of uPDF sets, we calculate the cross sections differential in either the transverse momentum of the Z boson or $\Delta\phi_{Zhb}$ (distance in polar angle between Z and $\max(p_{b\perp}, p_{\bar{b}\perp})$) using different sets of uPDFs, namely CCFM J2003 set 1, 2, 3 [26] and CCFM set A0 [27], which are all obtained from fits to HERA F_2 data [28]. In addition we use the unintegrated parton density by [20], referred to as KMR. The resulting plots are shown in Figs. 3.12 and 3.13. We do not show the distributions for set 1, because they are very close to distribution for the set 3, to keep the plot clear.

The total cross sections obtained for different uPDFs can be seen in Tab. 3.2. The

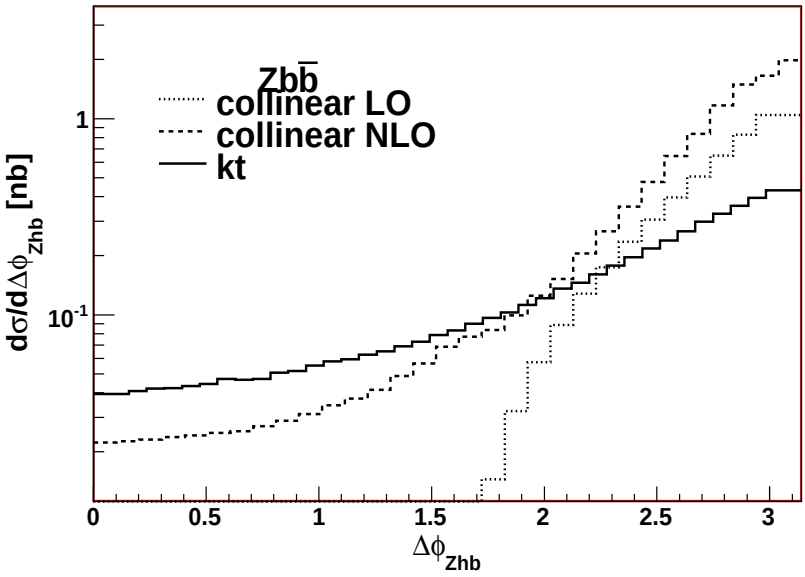

Figure 3.10: Comparison of cross sections differential in distance in azimuthal angle of Z and higher $p_\perp$ $b/\bar{b}$. Calculation with massless b-quarks. The applied cuts are described in the text.

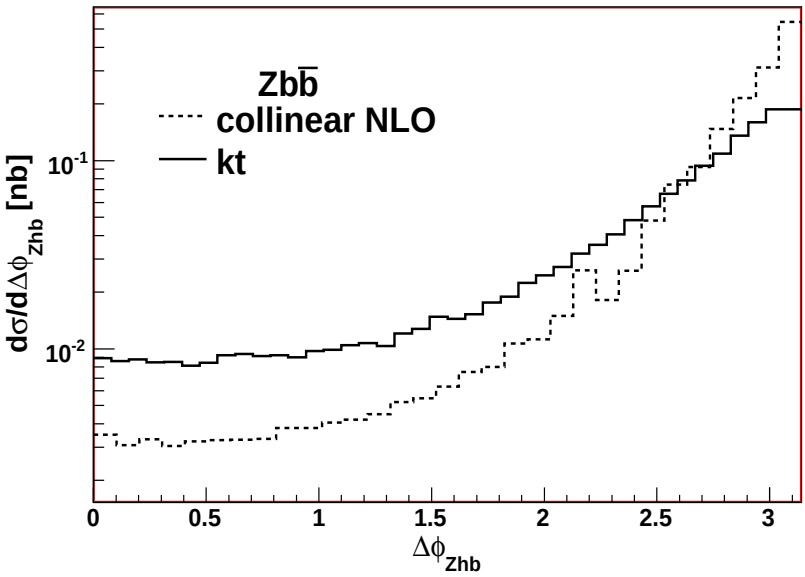

Figure 3.11: Comparison of cross sections differential in distance in azimuthal angle of Z and higher $p_\perp$ $b/\bar{b}$. Calculation with massless b-quarks. An additional cut on $p_{Z\perp} > 50\,\mathrm{GeV}$ has been applied.

uPDF	Total cross section [nb]
CCFM J2003 set 1	0.369
CCFM J2003 set 2	0.147
CCFM J2003 set 3	0.406
CCFM set B0	0.277
CCFM set A0	0.378
KMR	0.190

Table 3.2: Total cross sections of the process $pp \to Zb\bar{b}+X$ for different sets of unintegrated parton distribution functions.

μ_R	Total cross section [nb]
m_Z	0.406
$2m_Z$	0.392
$\frac{1}{2}m_Z$	0.607
$\sqrt{m_Z^2+p_{Z\perp}^2}$	0.467
$2\sqrt{m_Z^2+p_{Z\perp}^2}$	0.381
$\frac{1}{2}\sqrt{m_Z^2+p_{Z\perp}^2}$	0.585

Table 3.3: Total cross sections for different renormalization scale μ.

total cross section varies for these different uPDFs about 45%, while the shape of the distributions is hardly effected except of the KMR. KMR set uses completely different evolution equations and a deviation is not surprising.

As a last point to discuss, we turn to the scale dependence. As already mentioned in the beginning of section 3 the factorization scale is fixed by the emission angle of the hard subprocess. However, there is still freedom in choice of the renormalization scale which should be of order of the typical scale of the hard subprocess.

We consider two possible choices: the constant renormalization scale $\mu_1 = m_Z$ and the scale $\mu_2 = \sqrt{m_Z^2 + p_{Z\perp}^2}$, which are varied by factor of 2, so μ has values $2\mu_1$, $\frac{1}{2}\mu_1$ and $2\mu_2$, $\frac{1}{2}\mu_2$. The results for the $p_{Z\perp}$ and the $\Delta\phi_{Zhb}$ distribution can be seen in Figs. 3.14 and 3.15, respectively. The values of the cross section for individual choices of the scale are summarized in Tab. 3.3. One can see that a running α_S does not affect the shape of the distributions, but only the total cross section.

4 Summary and Conclusions

In this paper we have calculated the matrix element for the process $g^*g^* \to W/Zq_i\bar{q}_j$, taking into account the virtuality and transversal momenta of the initial gluons in the k_T-factorization formalism. We have implemented the matrix element squared in the Monte Carlo generator CASCADE and have calculated the total and differential cross sections of this process in proton proton collisions for the LHC at energy of $\sqrt{s} = 14$TeV. We have

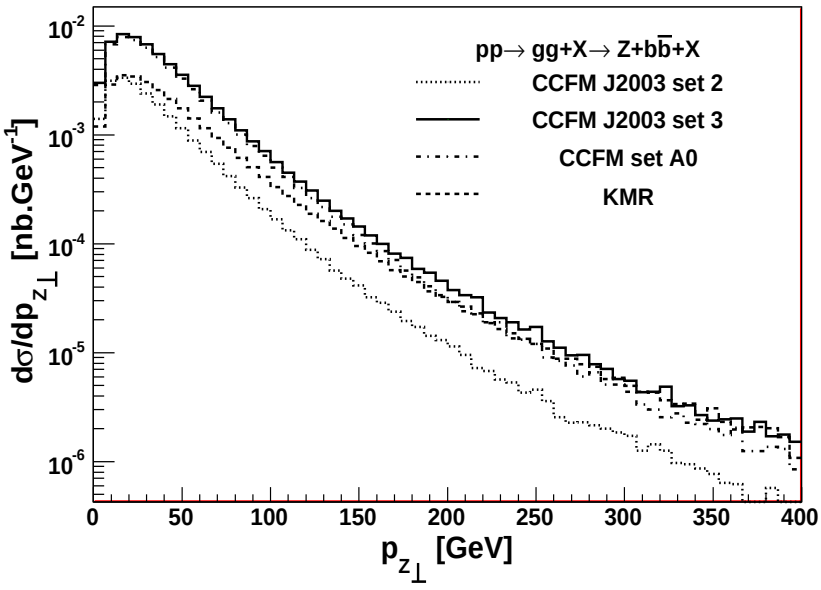

Figure 3.12: Transverse momentum distributions of produced Z gauge boson calculated in CASCADE using massive quarks. Cases with different uPDFs compared.

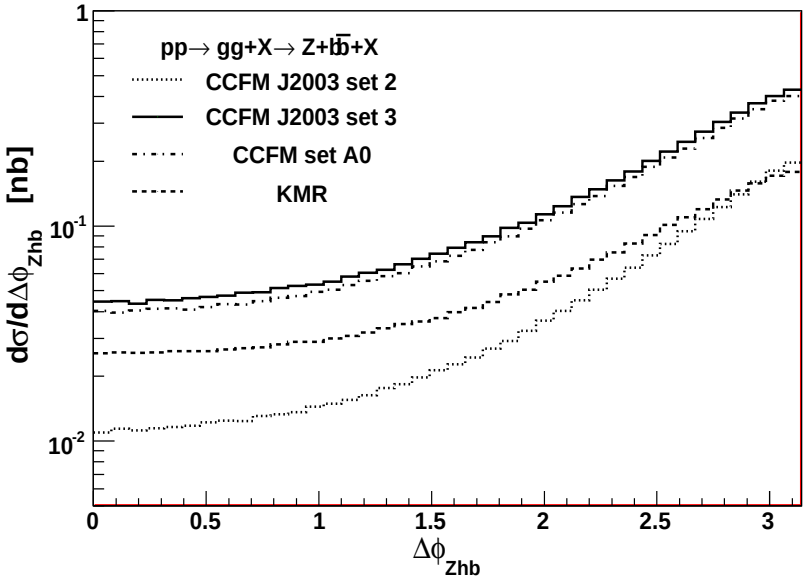

Figure 3.13: Comparison of cross sections differential in distance in azimuthal angle of Z and higher $p_\perp$ $b/\bar{b}$, using massive quarks. Cases with different uPDFs compared.

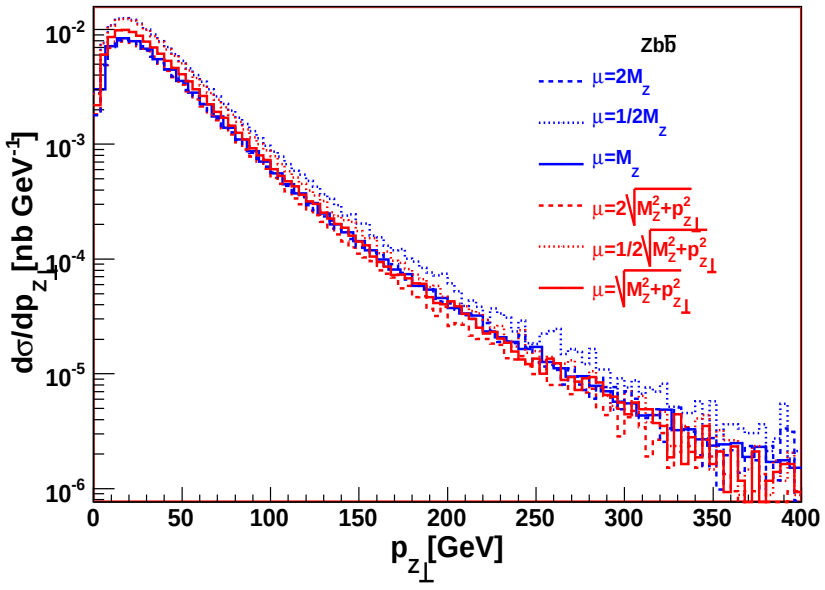

Figure 3.14: Transverse momentum distributions of produced Z gauge boson calculated in CASCADE using massive quarks. Cases with different renormalization scales μ_R compared.

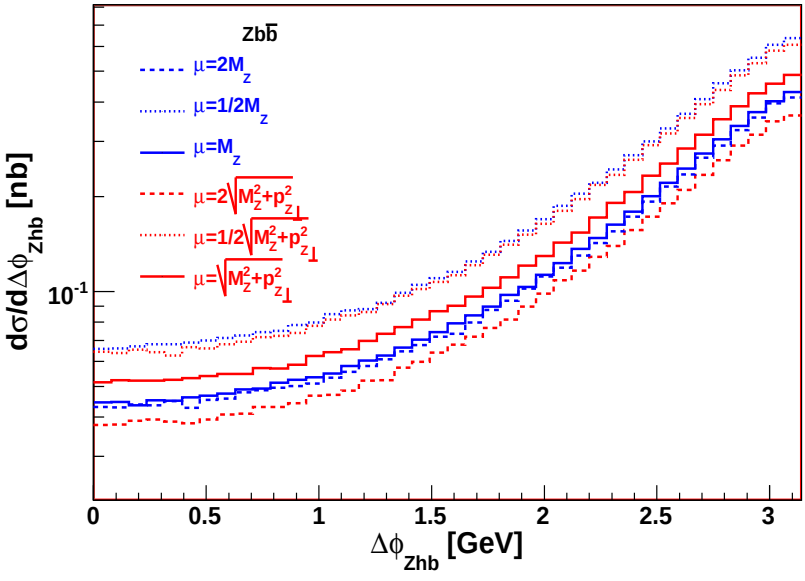

Figure 3.15: Transverse momentum distributions of produced Z gauge boson calculated in CASCADE using massive quarks. Cases with different renormalization scales μ_R compared.

compared our results with results obtained in collinear factorization (using MCFM). The total cross sections differ by a factor of ~ 2. There are differences in distributions which are sensitive to compensation of transversal momenta of particles in the final state coming from rather fundamental differences between the two approaches.

We found the most significant differences in the cross section differential in the azimuthal angle between the Z boson and higher p_T quark or antiquark – $\Delta\phi_{Zhb}$. While for a LO calculation in collinear factorization a region of values of $\Delta\phi_{Zhb}$ is kinematically forbidden, in k_T-factorization the whole range of $\Delta\phi_{Zhb}$ is allowed. This is because of neglecting the contribution of transversal momenta of initial state gluons in calculation of matrix element in collinear factorization. The NLO collinear calculation (where transversal momentum is generated by real corrections) shows already the same qualitative behavior as the k_T-factorization calculation. However, there remains a difference in the shape of the distribution of $\Delta\phi_{Zhb}$ compared to the k_T-factorization calculation We also compared cross sections differential in the transversal momentum of the $Zb\bar{b}$ system – $p_{Zb\bar{b}\perp}$. In collinear factorization and lowest order perturbation theory (α_S^2), the observable $p_{Zb\bar{b}\perp}$ is exactly zero. For a non-zero contribution in collinear factorization higher order corrections are needed. The k_T-factorization gives non-zero contribution already at α_S^2 order. We have compared cross sections differential in $p_{Zb\bar{b}\perp}$ calculated in NLO in collinear calculation and LO in k_T-factorization. The distributions have different shape at low values of $p_{Zb\bar{b}\perp}$. At high $p_{Zb\bar{b}\perp}$ the slopes are similar but differ in absolut size.

We have calculated the cross sections differential in the transversal momentum of the produced boson. The maximum of the distribution in the k_T-factorization calculation is at higher transversal momenta compared to the collinear one. This shows the sensitivity of this distribution on parton evolution model and treatment of kinematics.

We conclude that some of the effects of NLO and even higher order collinear calculation are already included in the LO k_T-factorization calculation.

Acknowledgments

First of all, we would like to thank H. Jung and J. Bartels for their help, advice, and support during all stages of this work. We would like to express special thanks to S. P. Baranov for useful advice and introduction to method of orthogonal amplitudes, which was crucial to obtain numerically stable results. We are thankful to J. Campbell for help with filling of histograms in Monte Carlo generator MCFM. We also benefited from interesting discussions with A. Bacchetta. F.S. has been supported in part by the Deutsche Forschungsgemeinschaft, DFG Grant No. GRK 602, and the Agence Nationale de la Recherche (France), contract No ANR-06-JCJC-0084-02. This work is associated with the DFG Collaborative Research Centre SFB 676.

References

[1] L. Agostino, L. Malgeri, G. Daskalakis, P. Govoni, and M. Paganoni, J. Phys. **G33**, N67 (2007);
J. D'Hondt, S. Lowette, J. Heyninck, and S. Kasselmann, CMS NOTE **025** (2006).

[2] M. Dittmar, F. Pauss, and D. Zurcher, Phys. Rev. **D56**, 7284 (1997) [hep-ex/9705004].

[3] V. N. Gribov and L. N. Lipatov, Sov. J. Nucl. Phys. **15**, 438 (1972);
L. N. Lipatov, Sov. J. Nucl. Phys. **20**, 94 (1975);
G. Altarelli and G. Parisi, Nucl. Phys. **B126**, 298 (1977);
Y. L. Dokshitzer, Sov. Phys. JETP **46**, 641 (1977).

[4] V. S. Fadin, E. A. Kuraev, and L. N. Lipatov, Phys. Lett. **B60**, 50 (1975);
E. A. Kuraev, L. N. Lipatov, and V. S. Fadin, Sov. Phys. JETP **44**, 443 (1976);
E. A. Kuraev, L. N. Lipatov, and V. S. Fadin, Sov. Phys. JETP **45**, 199 (1977);
I. I. Balitsky and L. N. Lipatov, Sov. J. Nucl. Phys. **28**, 822 (1978).

[5] M. Ciafaloni, Nucl. Phys. **B296**, 49 (1988);
S. Catani, F. Fiorani, and G. Marchesini, Phys. Lett. **B234**, 339 (1990);
S. Catani, F. Fiorani, and G. Marchesini, Nucl. Phys. **B336**, 18 (1990);
G. Marchesini, Nucl. Phys. **B445**, 49 (1995).

[6] S. Catani, M. Ciafaloni, and F. Hautmann, Nucl. Phys. **B366**, 135 (1991).

[7] J. C. Collins and R. K. Ellis, Nucl. Phys. **B360**, 3 (1991).

[8] L. V. Gribov, E. M. Levin, and M. G. Ryskin, Phys. Rept. **100**, 1 (1983);
E. M. Levin, M. G. Ryskin, Y. M. Shabelski, and A. G. Shuvaev, Sov. J. Nucl. Phys. **53**, 657 (1991).

[9] J. C. Collins and D. E. Soper, Nucl. Phys. **B193**, 381 (1981);
X. Ji, J.-p. Ma, and F. Yuan, Phys. Rev. **D71**, 034005 (2005) [hep-ph/0404183];
X. Ji, J.-P. Ma, and F. Yuan, Phys. Lett. **B597**, 299 (2004) [hep-ph/0405085];
J. C. Collins and A. Metz, Phys. Rev. Lett. **93**, 252001 (2004) [hep-ph/0408249];
A. Bacchetta, C. Bomhof, P. Mulders, and F. Pijlman, Phys.Rev. **D72**, 034030 (2005) [hep-ph/0505268].

[10] J. C. Collins and J.-W. Qui, Phys. Rev. **D75**, 114014 (2007) [hep-ph/0705.2141v2].

[11] S. P. Baranov, A. V. Lipatov, and N. P. Zotov, Phys.Rev. **D77**, 074024 (2008) [arXiv:0708.3560 [hep-ph]].

[12] S. P. Baranov, A. V. Lipatov and N. P. Zotov [arXiv:0805.2650 [hep-ph]].

[13] H. Jung, Comput. Phys. Commun. **143**, 100 (2002) [hep-ph/0109102];
H. Jung and G. P. Salam, Eur. Phys. J. **C19**, 351 (2001) [hep-ph/0012143].

[14] D. Binosi and L. Theussl, Comput. Phys. Commun. **161**, 76 (2004) [hep-ph/0309015].

[15] L. N. Lipatov, Sov. J. Nucl. Phys. **23**, 338 (1976).

[16] J. A. M. Vermaseren (2000) [math-ph/0010025].

[17] J. A. M. Vermaseren, Nucl. Phys. Proc. Suppl. **116**, 343 (2003) [hep-ph/0211297].

[18] S. P. Baranov and V. L. Slad, Phys.Atom.Nucl. **67**, 808 (2004) [hep-ph/0603090].

[19] J. R. Forshaw and A. Sabio Vera, Phys. Lett. **B440**, 141 (1998) [hep-ph/9806394];
B. R. Webber, Phys. Lett. **B444**, 81 (1998) [hep-ph/9810286];
G. P. Salam, JHEP **03**, 009 (1999) [hep-ph/9902324].

[20] M. A. Kimber, A. D. Martin, and M. G. Ryskin, Phys. Rev. **D63**, 114027 (2001) [hep-ph/0101348].

[21] J. Campbell and K. Ellis. http://mcfm.fnal.gov/;
J. Campbell and K. Ellis, Phys. Rev. D **65**, 113007 (2002) [hep-ph/0202176];
J. Campbell, K. Ellis, and D. Rainwatter, Phys. Rev. D **68**, 094021 (2003) [hep-ph/0308195].

[22] J. Pumplin, D. Stump, J. Huston, H. Lai, P. Nadolsky, and W. Tung, JHEP **0207**, 012 (2002).

[23] V. S. Fadin and L. N. Lipatov, Phys. Lett. **B429**, 127 (1998) [hep-ph/9802290];
M. Ciafaloni and G. Camici, Phys. Lett. **B430**, 349 (1998) [hep-ph/9803389].

[24] J. Bartels, A. Sabio Vera, and F. Schwennsen, JHEP **0611**, 051 (2006) [hep-ph/0608154].

[25] C. Balazs and C. P. Yuan, Phys. Rev. **D56**, 5558 (1997) [hep-ph/9704258];
R. K. Ellis and S. Veseli, Nucl. Phys. **B511**, 649 (1998) [hep-ph/9706526].

[26] M. Hansson and H. Jung (2003) [hep-ph/0309009].

[27] H. Jung (2004). [hep-ph/0411287].

[28] H1 Collaboration, S. Aid *et al.*, Nucl. Phys. **B470**, 3 (1996) [hep-ex/9603004];
H1 Collaboration, C. Adloff *et al.*, Eur. Phys. J. **C21**, 33 (2001) [hep-ex/0012053];
ZEUS Collaboration, M. Derrick *et al.*, Z. Phys. **C72**, 399 (1996) [hep-ex/9607002];
ZEUS Collaboration, S. Chekanov *et al.*, Eur. Phys. J. **C21**, 443 (2001) [hep-ex/0105090].